A Nearshore Oceanic Front Induced by Wave Streaming

PENG WANG,[a] JAMES C. MCWILLIAMS,[a] AND YUSUKE UCHIYAMA[b]

[a] *Department of Atmospheric and Oceanic Sciences, University of California, Los Angeles, Los Angeles, California*
[b] *Department of Civil Engineering, Kobe University, Kobe, Japan*

(Manuscript received 6 January 2021, in final form 23 March 2021)

ABSTRACT: Coastal fronts impact cross-shelf exchange of materials, such as plankton and nutrients, that are important to the ecosystems in continental shelves. Here, using numerical simulation we demonstrate a nearshore front induced by wave streaming. Wave streaming is a bottom Eulerian current along the surface wave direction, and it is caused by the wave bottom dissipation. Wave streaming drives a Lagrangian overturning circulation in the inner shelf and pumps up deep and cold water into the overturning circulation. The water inside the overturning circulation is quickly mixed and cooled because of the wave-streaming-enhanced viscosity. However, the offshore water outside the overturning circulation remains stratified and warmer. Hence, a front develops between the water inside and outside the overturning circulation. The front is unstable and generates submesoscale shelf eddies, which cause the offshore transport across the front. This study presents a new mechanism for coastal frontogenesis.

SIGNIFICANCE STATEMENT: Cross-shelf exchange of materials, such as plankton and nutrients, is important to the health of ecosystems in the continental shelves. Such material exchange is affected by various coastal fronts that are characterized by a sharp change of water properties (e.g., density, temperature, or salinity) in a narrow distance. Here we find a novel nearshore front caused by the bottom drag on surface waves. The front is located in water that is ~10 m deep, roughly parallel to the shore, and it extends from the surface to the bottom. The front acts as a barrier that limits the material transport across the front. However, the front is unstable and generates eddies spreading offshore. These eddies break the frontal barrier, causing the offshore transport across the front. This study presents a new mechanism for coastal frontogenesis.

KEYWORDS: Coastal flows; Frontogenesis/frontolysis; Fronts; Waves, oceanic

1. Introduction

The health of marine ecosystems in continental shelves relies on the cross-shelf exchange of materials, such as nutrients, pollutants, and plankton (Nittrouer and Wright 1994; Shanks et al. 2015; Fujimura et al. 2018). The cross-shelf exchange is controlled by numerous processes (Lentz and Fewings 2012; Brink 2016), and one of them is coastal fronts that are characterized by a sharp change of water properties (e.g., density, temperature, or salinity) in a narrow distance (McWilliams 2021). Fronts can act as a barrier that limits the cross-shelf exchange (Brink 2016). For example, Fig. 1 shows a nearshore front that is located at about 2 km from the shore, roughly parallel to the shoreline. The front gathers floating yellow algae into an alongshore band, limiting the cross-shelf dispersion of the algae.

There are several types of coastal fronts (McWilliams 2021). Along-shelf winds drive a cross-shelf Ekman transport, causing an upwelling or downwelling front (Allen et al. 1995; Austin and Lentz 2002). Tidal currents enhance vertical mixing in shallow water, resulting in a tidal mixing front that separates mixed shallow water from its surroundings (Simpson and Hunter 1974; Chen et al. 2003). Around a shelf break, cold fresh shelf water is separated from warm salty slope water by a shelf-break front (Houghton et al. 1988; Chapman and Lentz 1994; Gawarkiewicz et al. 2004). Internal waves can create fronts parallel to wave crests, and such fronts usually move with the waves (Shanks 1983; Pineda 1994).

Surface gravity waves affect oceanic frontogenesis (Suzuki et al. 2016; McWilliams 2018). Surface waves may sharpen or widen a front depending on the alignment between the front and Stokes drift (Suzuki et al. 2016; Sullivan and McWilliams 2019). Moreover, depth-induced wave breaking enhances vertical mixing in a surf zone (MacMahan et al. 2006; Reniers et al. 2009; Brown et al. 2015; Uchiyama et al. 2017; Akan et al. 2020; Wang et al. 2020); in contrast to the offshore weaker mixing, a front may occur around the surf-zone edge (Kumar and Feddersen 2017).

Surface waves also induce wave streaming that is a wave-averaged Eulerian current along the wave direction (Longuet-Higgins 1953). Wave streaming includes surface streaming and bottom streaming. The surface streaming is driven by a viscous stress with wave velocity shear in a wave surface boundary layer (Xu and Bowen 1994). Surface streaming may affect ocean surface transport and Langmuir circulation (Weber et al. 2006; Wang and Özgökmen 2018). The bottom streaming is driven by a stress due to wave velocity fluctuations in a wave bottom boundary layer (Longuet-Higgins 1953). The wave velocity fluctuations are generated when surface waves experience bottom drag in shallow water. Bottom streaming may be affected by asymmetric wave shapes (Trowbridge and Madsen 1984; Kranenburg et al. 2012). In this study we neglect the surface streaming because of its smallness (Uchiyama et al. 2010)

Corresponding author: Peng Wang, wangpeng@ucla.edu

DOI: 10.1175/JPO-D-21-0004.1

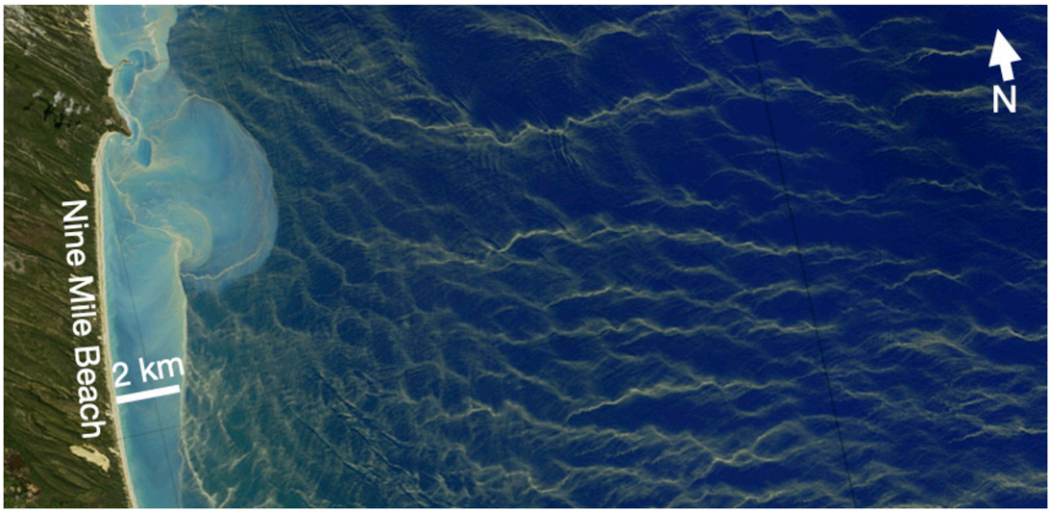

FIG. 1. A satellite image of algae (*Trichodesmium*) blooms off Nine Mile Beach, Queensland, Australia, on 15 Sep 2018. The image was collected by the USGS–NASA *Landsat-8* Operational Land Imager and distributed by the NASA Ocean Biology Processing Group. In the far offshore, yellow algae slicks are gathered into shore-normal windrows by Langmuir circulation. In the nearshore, yellow algae are accumulated into a shore-parallel band located at about 2 km from the shore. This algae band is more than 10 km alongshore in about 10 m-deep water (inner shelf), and it implies that there exists an alongshore front. The murky water between the shore and the algae band is likely due to strong mixing by surf eddies and inner-shelf currents.

and focus on the bottom streaming; hereinafter, "wave streaming" denotes the bottom streaming only.

Wave streaming affects inner-shelf circulation (Lentz et al. 2008; Wang et al. 2020), and it is crucial to the transport of sediments and near-bed fish larvae from the inner shelf to the surf zone (Reniers et al. 2004; Shanks et al. 2015; Fujimura et al. 2018). But roles of wave streaming in coastal frontogenesis remain unknown. Wang et al. (2020) report that wave streaming drives an inner-shelf Lagrangian overturning circulation in unstratified water. By extending that study to stratified water, we find that wave streaming induces a shore-parallel nearshore front, associated with the inner-shelf Lagrangian overturning circulation.

This study is organized as follows. The numerical model and experiment configurations are described in section 2. The experiment results are analyzed in section 3, such as the wave-streaming-induced circulation and front. Further, in section 4 the circulation and front are examined in various environments, including tides and winds. The study is summarized in section 5.

2. Methods

a. Numerical model

Numerical experiments are conducted with a coupled wave–circulation model (Uchiyama et al. 2010), which is a spectrum-peak surface wave model coupled with Regional Oceanic Modeling System (ROMS). This coupled model has been validated against field measurements of waves and currents (Uchiyama et al. 2010; Marchesiello et al. 2015). The wave model gives wave effects on currents (WEC) to the circulation model and, in turn, takes current effects on waves (CEW) from the circulation model. Taking CEW into account is crucial for a wave model to give accurate WEC, because CEW significantly modify waves and thereby WEC (Wang and Özgökmen 2018; Romero et al. 2020). The WEC are separated into conservative and nonconservative parts. The conservative part contains Stokes vortex force, Stokes–Coriolis force, and wave-induced pressure (McWilliams et al. 2004). The nonconservative part is parameterized, including wave breaking, wave streaming, and wave-enhanced bottom drag (see the appendix).

b. Experiment configuration

The numerical topography (Fig. 2a) is an idealized continental shelf, a sloping plane with a slope of 0.005 (≈0.3°). It is 25.6 km in the cross-shelf direction X and 20.48 km in the along-shelf direction Y, with a horizontal resolution of 40 m and 18 terrain-following layers. The water depth is 0.5 m at the shoreline and 128.5 m at the offshore boundary.

The initial water temperature is horizontally uniform and decreases with depth (Fig. 2b). The salinity is constant. The buoyancy frequency varies with depth (Fig. 2b) and represents a summertime stratification. Tides and winds are absent unless explicitly stated. Incident surface waves are prescribed at the offshore (eastern) open boundary. The western shoreline boundary is enforced with zero mass flux. The southern and northern boundaries are periodic. The K-profile parameterization (KPP; Large et al. 1994) is used for vertical mixing. The Coriolis parameter is $8.13 \times 10^{-5}\ \mathrm{s}^{-1}$ for a midlatitude. The experiment is simulated for 41 numerical days.

As explained by Wang et al. (2020), the incident waves are stochastic and mimic a spectrum-peak band of measured surface waves. The waves contain stochastic variations in the wave

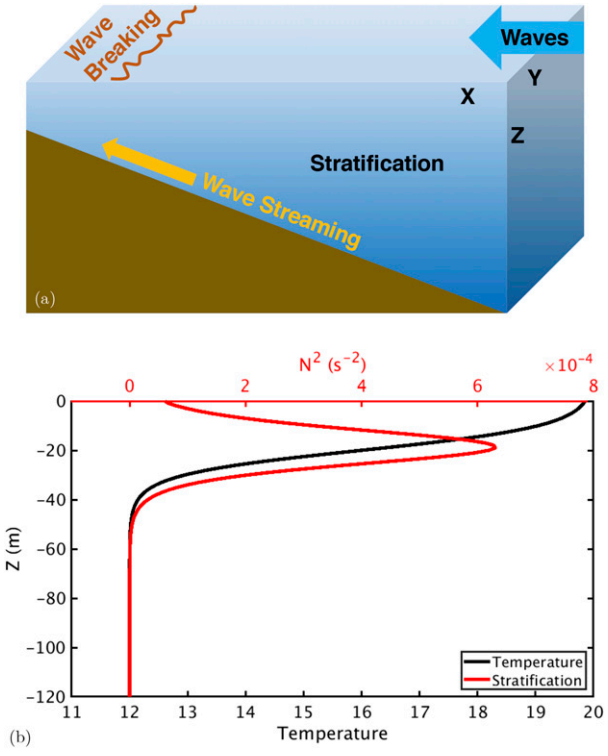

FIG. 2. (a) A schematic illustration of experiment configurations. (b) Initial profiles of temperature and stratification N^2.

height, period, and direction. The mean wave height is 0.8 m, the mean period is 10 s, and the mean direction is normal to the shore yet with a directional spread of 10°.

We focus on a nearshore region that consists of a surf zone and an inner shelf. The surf zone is where surface waves break due to shallow depth. Offshore next to the surf zone, the inner shelf is where surface and bottom boundary layers overlap (Nittrouer and Wright 1994; Lentz and Fewings 2012). In our experiment, however, the surface boundary layer does not exist owing to the absence of surface forcing. Instead, we refer to the inner shelf as where the bottom boundary layer roughly occupies the full depth next to the surf zone.

3. Results

a. Wave-streaming front

In the surf zone, depth-induced wave breaking is parameterized as a near-surface breaker force [Eq. (A2) in the appendix]. A pressure gradient force that balances the breaker force drives an offshore undertow. This undertow extends from the surf zone to the inner shelf (Fig. 3a; $x < 2$ km). There is also a bottom onshore current in the inner shelf (Fig. 3a; $0.5 < x < 2$ km). This current is wave streaming and is generated by a parameterized, near-bottom streaming force [Eq. (A4)].

We define a Lagrangian streamfunction ψ^L as

$$u^L = -\frac{\partial \psi^L}{\partial z} \quad \text{and} \quad w^L = \frac{\partial \psi^L}{\partial x}, \tag{1}$$

where u^L and w^L denote the cross-shelf and vertical Lagrangian velocity, respectively (Wang et al. 2020). The Lagrangian velocity is the sum of an Eulerian velocity and Stokes drift. The Lagrangian streamfunction reveals two overturning circulations located in the surf zone and inner shelf (Fig. 3b). In particular, the inner-shelf overturning circulation is driven by wave streaming (Wang et al. 2020), and it is narrower than its counterpart in unstratified water (Wang et al. 2020, their Fig. 6a).

Wave breaking and wave streaming enhance vertical eddy viscosity in the surf zone and inner shelf, respectively (Fig. 3c). The enhancement of eddy viscosity is incorporated into KPP (Uchiyama et al. 2010), including a bottom KPP. Interestingly, the viscosity enhanced by wave streaming appears largely inside the inner-shelf overturning circulation, significantly increasing the vertical mixing inside this circulation.

Wave streaming pumps up deep and cold water into the inner-shelf overturning circulation. Because of the enhanced viscosity, the water inside the overturning circulation is quickly mixed and cooled (Fig. 3d; $0.5 < x < 2$ km). By contrast, the offshore water outside the overturning circulation remains stratified and warmer (Fig. 3d; $x > 2$ km). Hence, a front develops between the water inside and outside the overturning circulation (Fig. 3d; $x \approx 2$ km). We call it the "wave-streaming front."

b. Frontogenetic tendency

The wave-streaming front is featured with large cross-shelf temperature gradients (Fig. 4a), which extend to the bottom along the downwelling (Fig. 3b, green arrow) beneath the surface front. The frontogenetic tendency expressed with the cross-shelf temperature gradient is diagnosed with the following equation:

$$\frac{D^L}{Dt}\left[\frac{1}{2}\left(\frac{\partial T}{\partial x}\right)^2\right] = \underbrace{\left(-\frac{\partial u}{\partial x}\frac{\partial T}{\partial x} - \frac{\partial v}{\partial x}\frac{\partial T}{\partial y}\right)\frac{\partial T}{\partial x}}_{F_{\mathrm{velH}}} + \underbrace{\left(-\frac{\partial w}{\partial x}\frac{\partial T}{\partial z}\right)\frac{\partial T}{\partial x}}_{F_{\mathrm{velV}}} + \underbrace{\left(-\frac{\partial u_j^s}{\partial x}\frac{\partial T}{\partial x_j}\right)\frac{\partial T}{\partial x}}_{F_{\mathrm{Stk}}} + \underbrace{\frac{\partial}{\partial x}\left[\frac{\partial}{\partial x_j}\left(\kappa\frac{\partial T}{\partial x_j}\right)\right]\frac{\partial T}{\partial x}}_{F_{\mathrm{mix}}}. \tag{2}$$

Equation (2) is derived by taking the derivative $\partial/\partial x$ of the advection–diffusion equation for temperature with Stokes drift included, and then multiplying it by $\partial T/\partial x$ (Hoskins 1982; McWilliams 2021). The operator $D^L/Dt = \partial/\partial t + (\mathbf{u}^L \cdot \nabla)$ is a total derivative with Lagrangian velocity $\mathbf{u}^L$, κ is the temperature diffusivity, and $j = 1, 2, 3$. The l.h.s. of Eq. (2) is the frontogenetic tendency. A positive or negative frontogenetic tendency respectively means that temperature gradients across the front will be intensified or reduced with time. The r.h.s. of Eq. (2) is grouped as follows: F_{velH} is strain by horizontal Eulerian velocity (u, v), F_{velV} is strain by vertical Eulerian velocity w, F_{Stk} is strain by Stokes drift (u^s, v^s, w^s), and F_{mix} is due to differential mixing.

The strains of Eulerian current F_{velH} (Fig. 4b) and F_{velV} (Fig. 4c) are the largest terms, yet the two compete with each other. Differential mixing F_{mix} is also significant, especially for

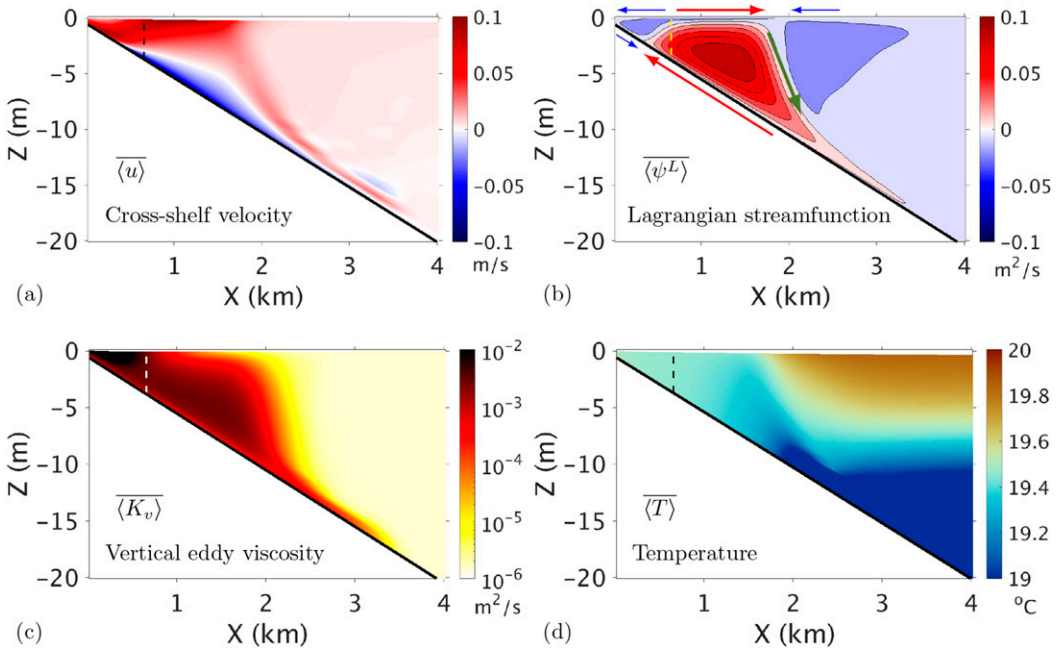

FIG. 3. (a) Cross-shelf Eulerian velocity. (b) Lagrangian streamfunction defined in Eq. (1). The arrows indicate directions of Lagrangian currents. (c) Vertical eddy viscosity. (d) Temperature. The angle brackets with overbar indicate averaging over both time and alongshore. A temporal average is made over the second day. The dashed lines mark the surf-zone edge.

the near-bottom frontogenetic tendency (Fig. 4d). Nevertheless, the Stokes drift effect F_{Stk} is weaker by a factor of $O(10)$ than others and therefore is neglected. Hence, the frontogenetic tendency here is determined by net effects of Eulerian current and mixing (Fig. 4e), and it indicates that the surface front is intensified with time while the bottom front is reduced. Intensification of the surface front may destabilize the front, leading to a frontal instability.

c. *Frontal instability*

In the surf zone, alongshore-variable wave breaking generates surf eddies (Fig. 5a, inset); they can burst out of the surf zone and reach and perturb the wave-streaming front at $x \approx 2$ km. About 5 days later, the front destabilizes at the surface and generates small eddies of $O(100)$ m with Rossby number $\mathrm{Ro} \equiv |\zeta|/f \sim 5$ (Fig. 5a; $x \approx 3$ km). While spreading offshore (Figs. 5b,c), these eddies grow bigger to $O(1)$ km with Ro of approximately 2. We call the offshore eddies generated by the front "shelf eddies."

The offshore spreading of shelf eddies is further demonstrated by eddy kinetic energy (EKE) in a Hovmöller diagram (Fig. 5d). Offshore from the front ($x > 2$ km), EKE grows with time and spreads over the shelf. The offshore EKE is largely confined within the top 10 m (Fig. 5e; $x > 3$ km). Especially at the front ($x \approx 2$ km), EKE concentrates at the surface rather than through full depth; this is consistent with the result that the frontal instability occurs at the surface.

From wave-averaged momentum equations that include wave forces (Uchiyama et al. 2010; Suzuki and Fox-Kemper 2016), we derive the following EKE equation:

$$\begin{aligned}\frac{\overline{D^L}}{Dt}\left(\frac{1}{2}\overline{u_i'^2}\right) = {} & \underbrace{\left(-\overline{u_i' u_j'^L}\frac{\partial \overline{u}_i}{\partial x_j}\right)}_{W_{\mathrm{flow}}} + \underbrace{\overline{w'b'}}_{W_{\mathrm{buoy}}} + \underbrace{\overline{(-f\hat{\mathbf{k}}\times\mathbf{u}^{s'})_i u_i'}}_{W_{\mathrm{StkCor}}} + \underbrace{\left[-\overline{\left(u_j\frac{\partial u_i^s}{\partial x_i}\right)' u_i'}\right]}_{W_{\mathrm{Stk}}} + \underbrace{\overline{F_i^{b'} u_i'}}_{W_{\mathrm{brk}}} + \underbrace{\overline{F_i^{f'} u_i'}}_{W_{\mathrm{strm}}} + \underbrace{\left(-\nu\overline{\frac{\partial u_i'}{\partial x_j}\frac{\partial u_i'}{\partial x_j}}\right)}_{W_{\mathrm{diss}}} \\ & + \underbrace{\frac{\partial}{\partial x_i}\overline{\left(-\frac{p'}{\rho_0}u_i'\right)} + \frac{\partial}{\partial x_j}\left[-\overline{u_j'^L\left(\frac{1}{2}u_i'^2\right)}\right] + \frac{\partial}{\partial x_i}\left[\overline{(u_j^s u_j)' u_i'}\right] + \frac{\partial}{\partial x_j}\left[\nu\frac{\partial}{\partial x_j}\left(\frac{1}{2}\overline{u_i'^2}\right)\right]}_{W_{\mathrm{trans}}}\end{aligned} \tag{3}$$

Again, the operator $D^L/Dt = \partial/\partial t + (\mathbf{u}^L \cdot \nabla)$ is a total derivative with Lagrangian velocity $\mathbf{u}^L$. The eddy component is denoted by the prime symbol and is defined as deviation from the alongshore average; for example, $u_i' = u_i - \langle u_i \rangle$, where angle

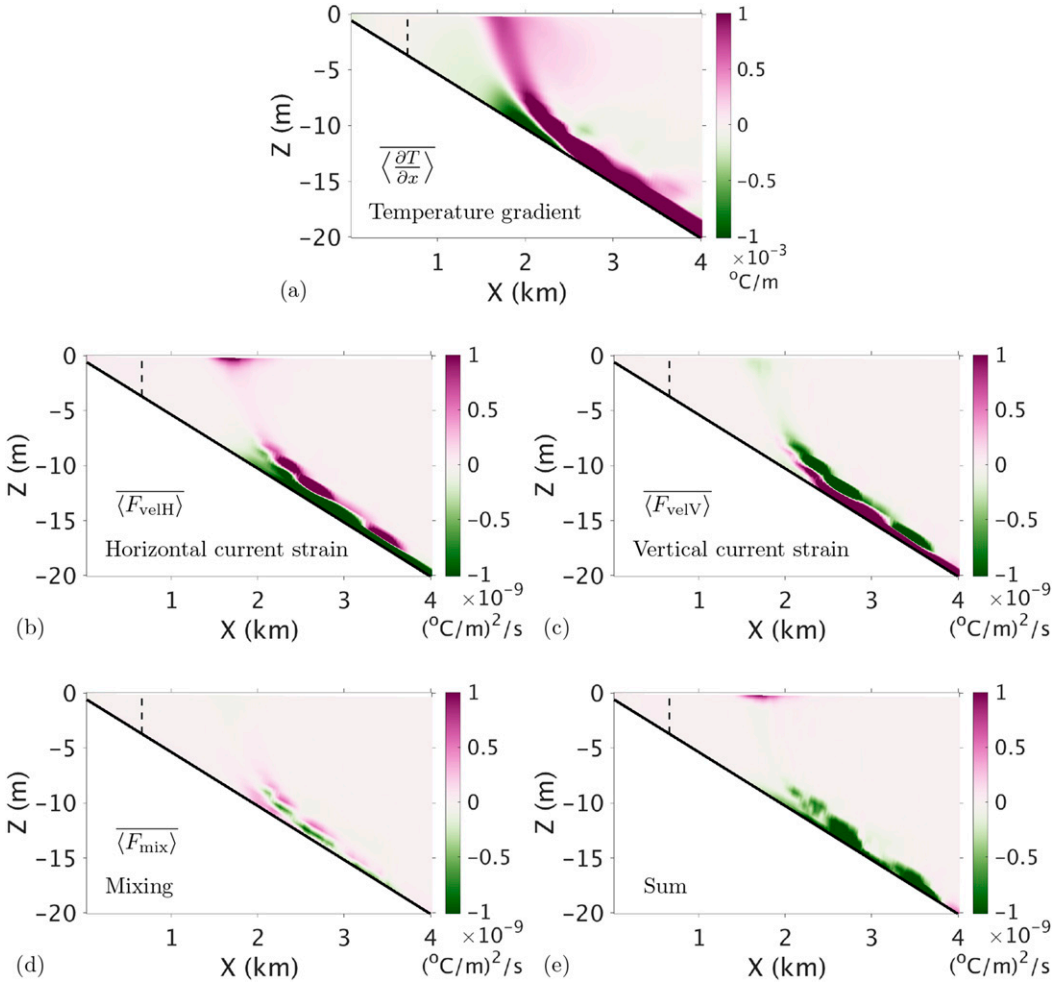

FIG. 4. (a) Cross-shelf temperature gradient. Also shown are the r.h.s. terms of Eq. (2) for frontogenetic tendency: (b) strain by horizontal Eulerian velocity, (c) strain by vertical Eulerian velocity, and (d) differential mixing. (e) The sum of the terms in (b)–(d). A temporal average is made over the second day. The dashed lines mark the surf-zone edge.

brackets denote an alongshore average. The overline above each term denotes a temporal average. The r.h.s. of Eq. (3) are grouped as follows:

- W_{flow} is mean-flow shear production, including horizontal shear $\left(\frac{\partial \overline{u}_i}{\partial x}, \frac{\partial \overline{u}_i}{\partial y}\right)$ and vertical shear $\left(\frac{\partial \overline{u}_i}{\partial z}\right)$;
- W_{buoy} is buoyancy b' production;
- W_{StkCor} is work by Stokes–Coriolis force $-f\hat{\mathbf{z}} \times \mathbf{u}^{s'}$;
- W_{Stk} is work by Stokes shear force[1] $\left(-u_j \frac{\partial u_j^s}{\partial x_i}\right)' = \left(-u_j \frac{\partial u_j^s}{\partial x_i}\right) - \left\langle -u_j \frac{\partial u_j^s}{\partial x_i} \right\rangle$;
- W_{brk} is work by wave-breaker force $F_i^{b'} = F_i^b - \langle F_i^b \rangle$ [appendix Eq. (A2)];
- W_{Strm} is work by wave-streaming force $F_i^{f'} = F_i^f - \langle F_i^f \rangle$ [Eq. (A4)];
- W_{diss} is turbulence dissipation;
- W_{trans} is divergence of EKE transport by turbulence.

Equation (3)'s r.h.s. contains four terms related to wave forces, namely, W_{StkCor}, W_{Stk}, W_{brk}, and W_{Strm}. The first two are linked to Stokes drift, and the last two arise from wave dissipation. These four terms represent wave effects on EKE and are primary energy passages from waves to currents.

In addition to the above four wave-related terms, there is another one in the mean-flow shear production W_{flow}, that is, the Stokes-drift-modified Reynolds stress $\overline{u_i' u_j^{L'}} = \overline{u_i' u_j'} + \overline{u_i' u_j^{s'}}$. The term $\overline{u_i' u_j^{s'}}$ is generally nonzero because u' and $u^{s'}$ are correlated by wave–current interaction. This Reynolds stress around the front is enhanced by surf eddies that reach the front. The enhanced Reynolds stress then amplifies the shear production at the front, accelerating frontal instability.

[1] Here the Stokes shear force is defined as $[-u_j(\partial u_j^s/\partial x_i)]$, slightly different than the Suzuki and Fox-Kemper (2016) definition of $[-u_j^L(\partial u_j^s/\partial x_i)]$ because of different algebraic manipulations.

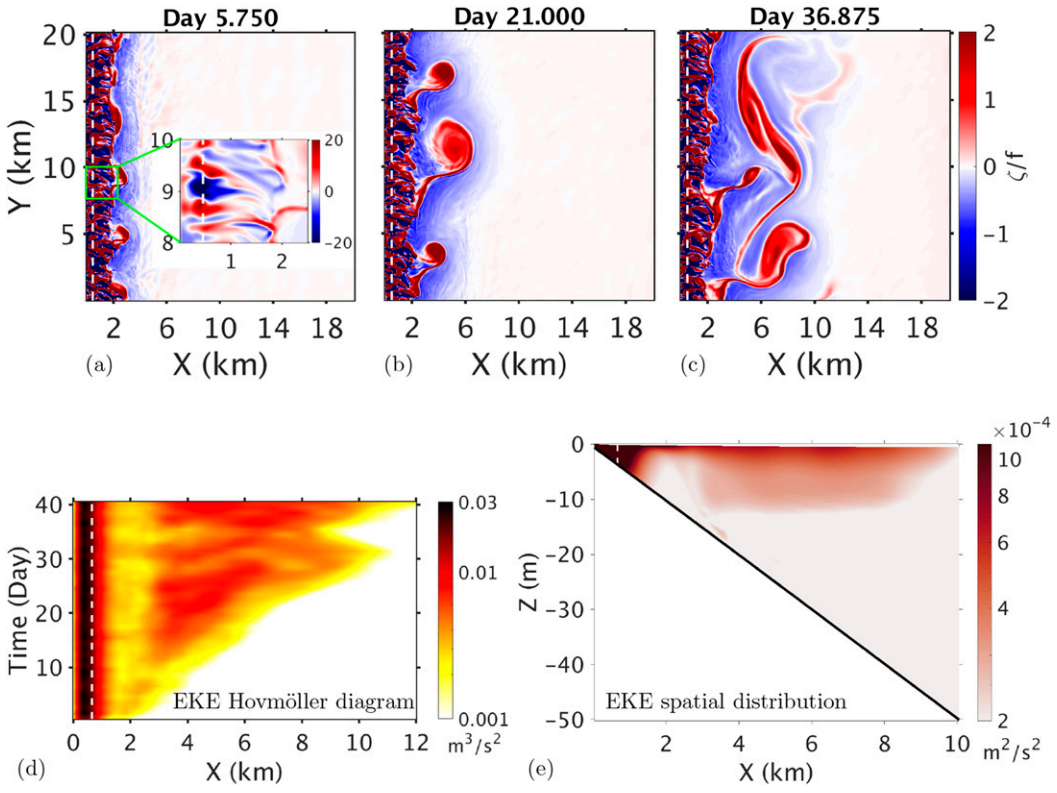

FIG. 5. (a)–(c) Evolution of the surface vertical vorticity normalized by the Coriolis parameter. (d) Hovmöller diagram of EKE (per unit mass) integrated over the depth and averaged alongshore. (e) EKE averaged over the last 10 days and alongshore. The dashed lines mark the surf-zone edge.

Most positive mean-flow shear work W_{flow} appears near the surface front (Fig. 6b; $x < 2.5$ km), while negative work appears near the inner-shelf bottom (Fig. 6b; $1 < x < 3$ km). A close examination decomposes the shear work into work by the horizontal shear and vertical shear. Specifically, it is the horizontal shear, instead of vertical shear, that makes the total shear work negative near the bottom. On the other hand, the horizontal shear is a leading contributor to the positive total shear work near the surface.

Large buoyancy production W_{buoy} around the front (Fig. 6a; $2 < x < 2.5$ km) supplies energy to the growth of frontal instability that evolves to shelf eddies. Besides, within the top 10 m offshore from the front (Fig. 6a; $3 < x < 5$ km), there exists another important buoyancy production that sustains the growth and offshore spreading of shelf eddies.

Stokes shear work W_{Stk} is significant near the surface front where the Stokes shear is strong (Fig. 6c). However, there the surface current is directed against the Stokes drift, making Stokes shear work compete with mean-flow shear work (Suzuki and Fox-Kemper 2016). Here the negative Stokes shear work removes EKE and weakens frontal instability, opposing the positive mean-flow shear work near the surface.

Wave-streaming work W_{Strm} is confined to the inner-shelf bottom because of the rapid decay of streaming force away from the bottom (Fig. 6d). Nonetheless, the frontal instability and shelf eddies largely appear near the surface away from the bottom (Fig. 5e; $x > 2$ km). Hence, the wave-streaming work is not considered to be a major energy source for the frontal instability and shelf eddies.

In brief, the shear production (W_{flow}) and buoyancy production (W_{buoy}) are major energy sources for the frontal instability and shelf eddies (Fig. 6e). This indicates that the frontal instability is a mixed barotropic–baroclinic instability (Cushman-Roisin and Beckers 2011).

Further, rotation is essential to the development of baroclinic instability (Cushman-Roisin and Beckers 2011), which makes the deformation radius relevant to the size of shelf eddies. Here the deformation radius[2] is about 1.23 km, close to the shelf-eddy size. In a comparison experiment without rotation, wave streaming still induces an inner-shelf overturning circulation and an associated front, similar to the case with rotation. But without rotation the front is stable and does not generate shelf eddies. Moreover, with rotation there is an alongfront current roughly in geostrophy, but without rotation this current disappears.

[2] The deformation radius is estimated as Nh/f with the buoyancy frequency $N = 0.01\ \text{s}^{-1}$, frontal height $h = 10$ m, and Coriolis parameter $f = 8.13 \times 10^{-5}\ \text{s}^{-1}$.

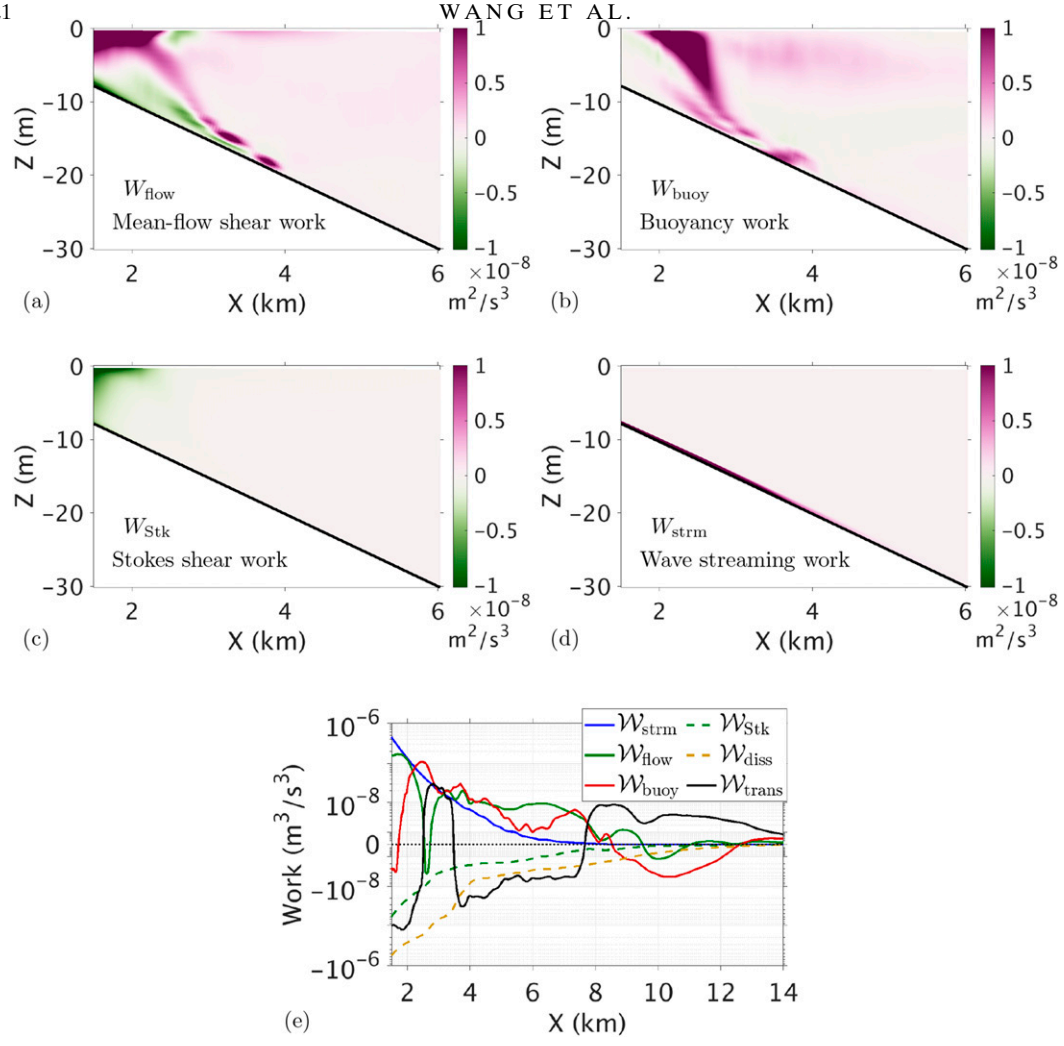

FIG. 6. The r.h.s. terms of Eq. (3) for eddy kinetic energy (per unit mass): work by (a) mean-flow shear, (b) buoyancy, (c) Stokes shear force, and (d) wave-streaming force. (e) Depth integrals of Eq. (3)'s r.h.s. terms. Note that the terms W_{StkCor} and W_{brk} are not shown in this plot because W_{StkCor} is too small and W_{brk} diminishes outside the surf zone. A temporal average is made over the last 10 days.

d. Cross-shelf transport

We use shore-released passive tracers to examine how the wave-streaming front (Fig. 7a) affects the cross-shelf transport. The tracers are governed by an advection–diffusion equation, in which the Stokes-drift advection is added (McWilliams et al. 2004; Uchiyama et al. 2010). Passive tracers are released in the shore-side water at the beginning of simulation. The initial tracer concentration in water shallower than 0.6 m is uniform and equals to 1 (dimensionless), and no tracer is released in the rest of water. Such tracers may represent plankton, nutrients, and pollutants in the surf zone.

The shore-released tracers are rapidly mixed within the surf zone (Fig. 7b; $x < 0.5$ km) owing to the wave-breaking-enhanced viscosity. Meantime, tracers are transported out of the surf zone into the inner shelf ($0.5 < x < 2$ km) by the mean Lagrangian current (Fig. 7c) and surf eddies (Fig. 7d).

Surface tracers are subducted at the front by the downwelling. One part (~65%) of the subducted tracers is then sent back to the surf zone by the bottom onshore mean Lagrangian current (Fig. 7c; $0.5 < x < 3$ km). The other part (~35%) is farther dispersed offshore mainly by shelf eddies (Fig. 7d; $x > 3$ km). In other words, shelf eddies cause the offshore transport across the front.

Because of the mutual advection by frontal downwelling and shelf eddies, tracers that cross the front into the offshore are concentrated below the surface about 10 m deep (Fig. 7b; $x > 3$ km). In unstratified water (no front), Wang et al. (2020) do not observe such offshore transport centered below the surface.

4. Discussion

The nearshore region is a complex environment that includes various dynamical processes and topography. Hence, it is necessary to explore how the wave-streaming-induced overturning circulation and front may be modified by various environments, such as topography, tides, and winds.

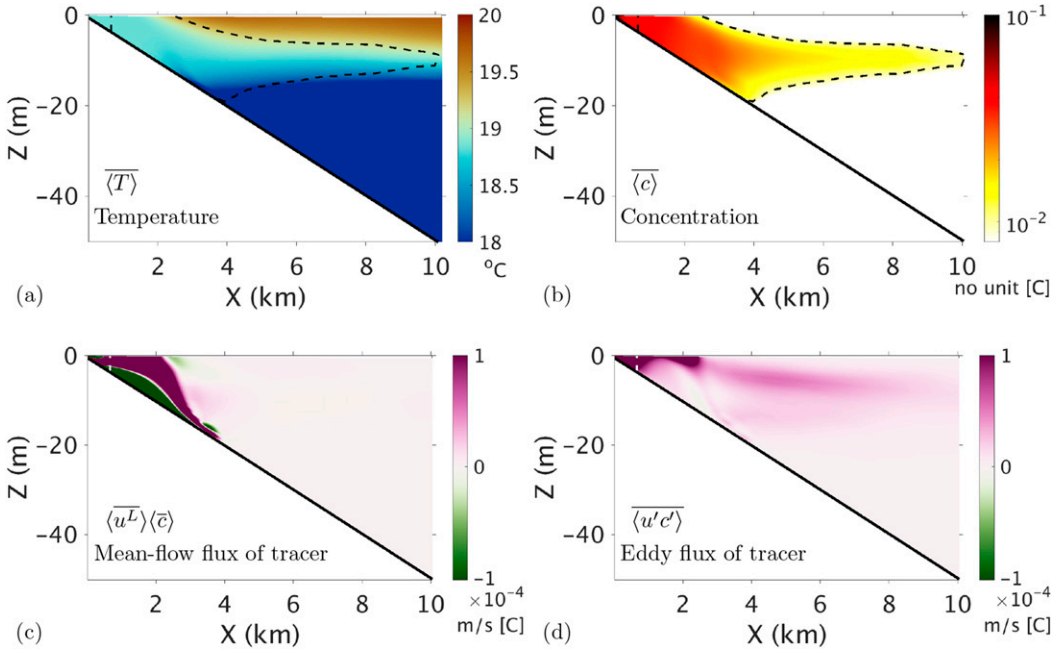

FIG. 7. (a) Temperature. Here the late-stage surface front is a few hundreds of meters wider than its early stage (Fig. 3d) but remains at similar strength. The curved dashed line is a contour of tracer concentration $\langle \overline{c} \rangle = 0.01$ (no units), and it roughly follows an isotherm (isopycnal). (b) Concentrations of shore-released passive tracers. The curved dashed line is the same as in (a). Also shown are cross-shelf tracer flux by the (c) mean Lagrangian currents and (d) eddies. A temporal average is made over the last 10 days. The vertical dashed lines mark the surf-zone edge.

a. Sensitivity of wave-streaming front

Sensitivities of the wave-streaming front are examined against wave energy, bottom roughness, shelf slope, and stratification, as they can affect the front via the parameterized streaming force [Eq. (A4) in the appendix].

1) WAVE ENERGY

We use wave height as a proxy of wave energy. In this study the offshore incident waves have a default mean height of 0.8 m. Now we use two additional mean wave heights of 0.4 and 1.2 m that represent smaller and bigger wave energy, respectively. The wave-streaming-induced overturning circulation (Figs. 8a,b) and front (Figs. 8c,d) can occur with either smaller or bigger waves but are different in size, strength, and location.

The surf zone is wider with bigger waves (Fig. 8b; $x < 1$ km) than with smaller waves (Fig. 8a; $x < 0.3$ km), because depth-induced breaking of bigger waves begins at a farther offshore location. Moreover, bigger waves induce a stronger breaker force [Eq. (A2)] and thereby drive a stronger surf-zone circulation (Fig. 8b) than smaller waves do (Fig. 8a).

Bigger waves also induce a stronger streaming force [appendix Eq. (A4)] and thus generate stronger wave streaming than smaller waves do (Fig. 8e). The wave streaming with bigger waves starts at a farther offshore location; thus, it drives a wider and stronger inner-shelf overturning circulation (Fig. 8b) than the streaming with smaller waves does. Namely, as wave energy increases, the inner-shelf overturning circulation expands offshore and pushes the front offshore (Fig. 8f). Furthermore, the wave streaming with bigger waves pumps up deeper and colder water, making the nearshore water with bigger waves cooler (Fig. 8d) than that with smaller waves (Fig. 8c).

2) BOTTOM ROUGHNESS

Sea bed roughness is measured by a bottom roughness height. In this study the default bottom roughness height is $z_o = 10^{-3}$ m, commonly used in nearshore ocean simulations. Now we use two additional bottom roughness heights of $z_o = 10^{-4}$ m and $z_o = 10^{-2}$ m that represent smooth and rough beds, respectively. The wave-streaming-induced overturning circulation (Figs. 9a,b) and front (Figs. 9c,d) can form above either a smooth or a rough bed but differs in size, strength, and location.

Before depth-induced breaking, wave energy is dissipated by bottom drag first. Less wave energy is removed by bottom dissipation above a smooth bed than above a rough bed; thus, more wave energy is left for breaking above a smooth bed, leading to a stronger surf-zone circulation (Fig. 9a). In fact, in this rough-bed case nearly all the wave energy is dissipated by bottom drag, making wave breaking trivial; thus, there is no surf zone or related circulation (Fig. 9b).

Wave streaming is stronger and starts at a farther offshore location above a rough bed than above a smooth bed (Fig. 9e). Hence, the wave streaming above a rough bed drives a stronger and wider inner-shelf overturning circulation (Fig. 9b) than it does above a smooth bed (Fig. 9a). Namely, as bed roughness increases, the inner-shelf overturning circulation expands offshore, pushing the front offshore (Fig. 9f). Furthermore, the

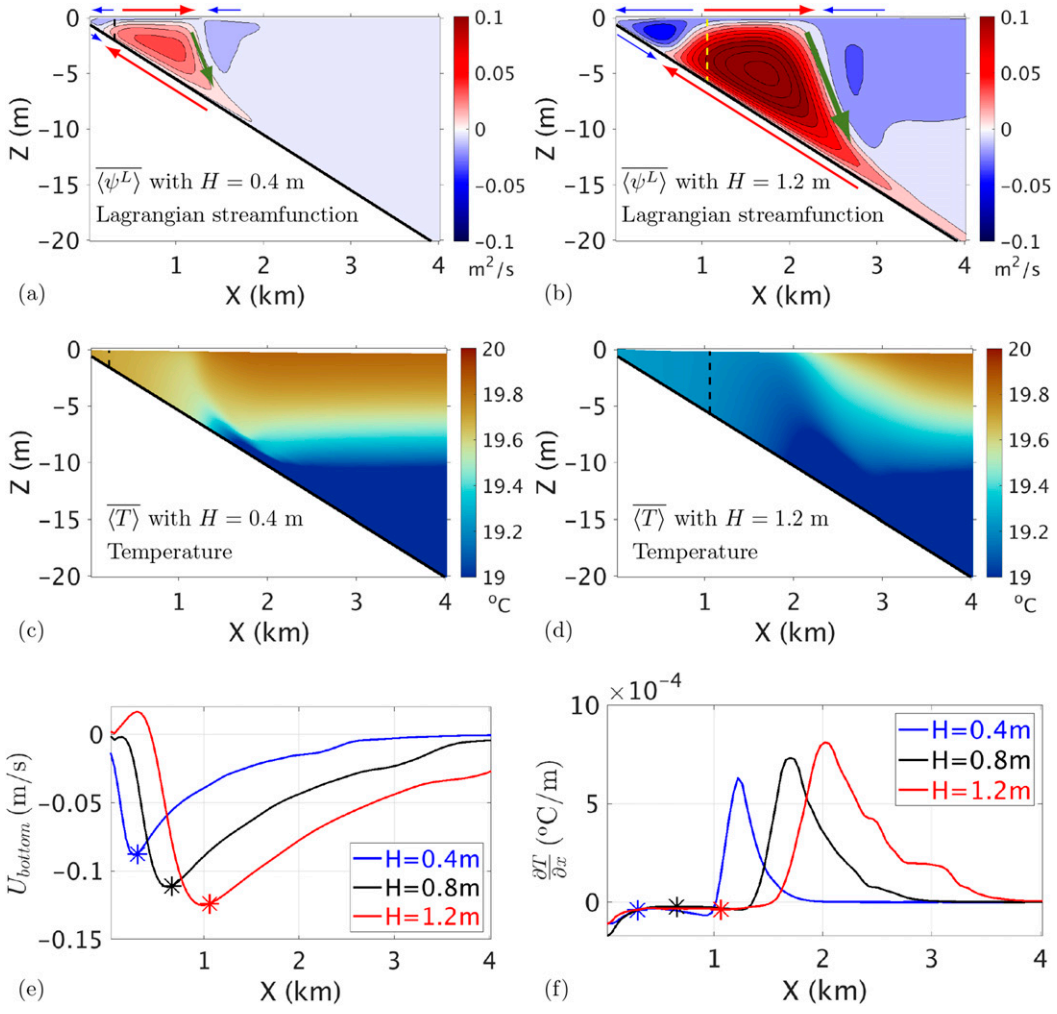

FIG. 8. Sensitivity to wave energy: Lagrangian streamfunction with wave height H = (a) 0.4 and (b) 1.2 m. The arrows indicate directions of Lagrangian currents. Temperature with H = (c) 0.4 and (d) 1.2 m. Alongshore-averaged (e) bottom cross-shelf Eulerian velocity and (f) surface cross-shelf temperature gradient. A temporal average is made over the second day. The dashed lines in (a)–(d) and the asterisks in (e) and (f) mark the surf-zone edge.

wave streaming above a rough bed brings up deeper and colder water, making the nearshore water above a rough bed cooler (Fig. 9d) than that above a smooth bed (Fig. 9c).

3) SHELF SLOPE

Shelf slopes affect the locations where wave breaking and streaming start. In this study the default shelf slope is 0.005. Now we use two additional shelf slopes of 0.0025 and 0.01 that represent gentle and steep shelves, respectively. The wave-streaming-induced overturning circulation (Figs. 10a,b) and front (Figs. 10c,d) can form in either a gentle or a steep shelf but vary in size, strength, and location.

The location where surface waves begin to experience bottom drag is farther offshore in a gentle shelf than in a steep shelf. Thus, wave streaming starts farther offshore in a gentle shelf, leading to a wider inner-shelf overturning circulation (Fig. 10a) than that in a steep shelf (Fig. 10b). Namely, as shelf slopes increase, the starting location of wave streaming shifts onshore (Fig. 10e). This narrows the inner-shelf overturning circulation, pulling the front onshore (Fig. 10f).

The distance over which surface waves experience bottom drag is shorter in a steep shelf than in a gentle shelf. Hence, less wave energy is removed by bottom dissipation in a steep shelf, and more energy is left for depth-induced breaking. This yields a stronger surf-zone circulation in a steep shelf (Fig. 10b) than that in a gentle shelf (Fig. 10a). Moreover, the surf zone is narrower in a steep shelf (Fig. 10b; $x < 0.3$ km) than in a gentle shelf (Fig. 10a; $x < 0.7$ km), because waves in a steep shelf have to be closer to the shore in order to trigger breaking caused by shallow depth.

A realistic shelf slope usually varies with locations. By mimicking the shelf shown in Fig. 1, we adopt a variable shelf slope that decreases from 0.02 in the surf zone to 0.002 in the far offshore. In this more realistic shelf, wave streaming is still

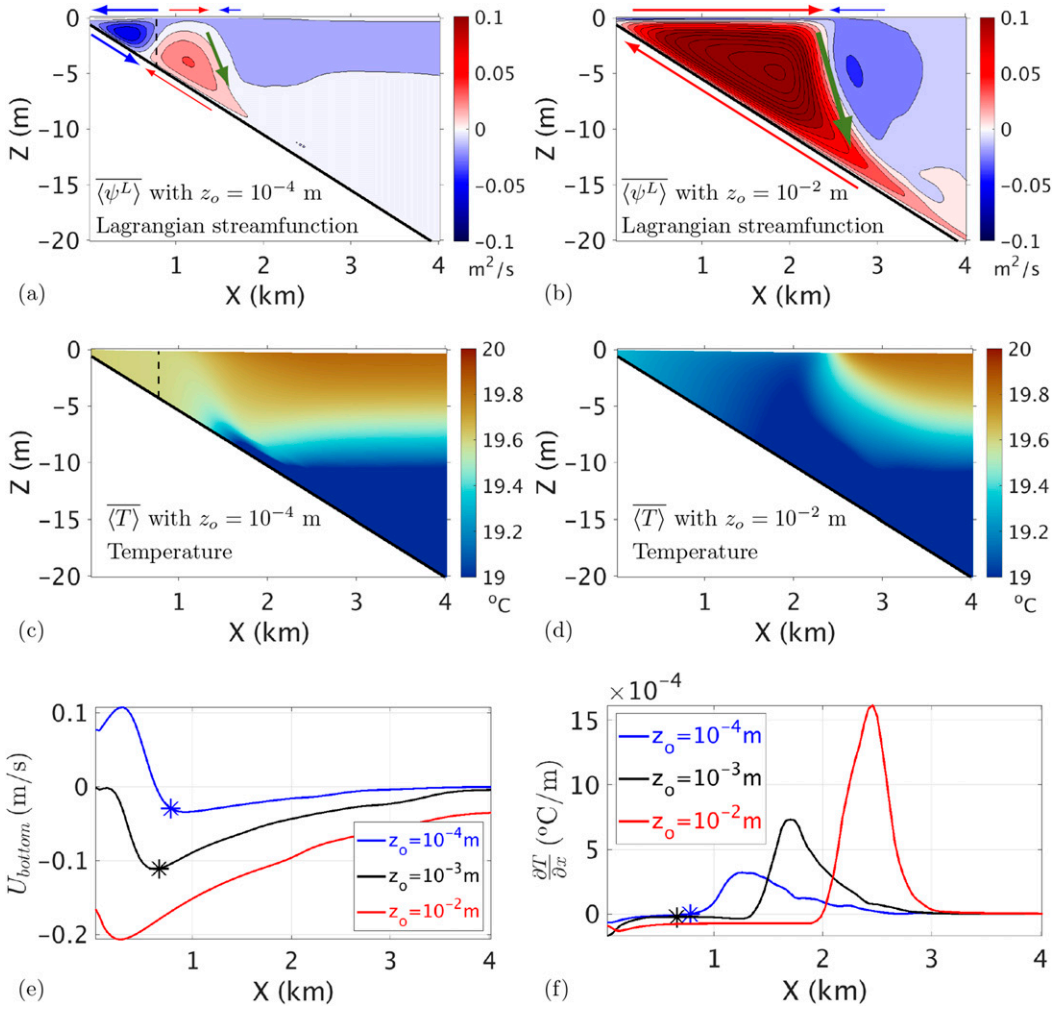

FIG. 9. Sensitivity to bottom roughness: Lagrangian streamfunction with bottom roughness height z_o = (a) 10^{-4} and (b) 10^{-2} m. The arrows indicate directions of Lagrangian currents. Temperature with bottom roughness height z_o = (c) 10^{-4} and (d) 10^{-2} m. Alongshore-averaged (e) bottom cross-shelf Eulerian velocity and (f) surface cross-shelf temperature gradient. A temporal average is made over the second day. The dashed lines in (a) and (c) and the asterisks in (e) and (f) mark the surf-zone edge. In this rough-bed case ($z_o = 10^{-2}$ m), wave breaking is trivial and thus no surf zone is identified.

able to drive an inner-shelf overturning circulation (Fig. 10g) and an associated front (Fig. 10h), showing the robustness of these wave-streaming-induced phenomena.

4) STRATIFICATION

For simplicity, we now use a linear and depth-uniform stratification, rather than the depth-dependent one shown in Fig. 2b. Three kinds of initial stratification are used, namely, $N^2 = 0.25 \times 10^{-4}\,\mathrm{s}^{-2}$, $1 \times 10^{-4}\,\mathrm{s}^{-2}$, and $4 \times 10^{-4}\,\mathrm{s}^{-2}$. The wave-streaming-induced overturning circulation (Figs. 11a,b) and front (Figs. 11c,d) take place in all cases but are different in size, strength, and location.

As stratification increases, the inner-shelf overturning circulation is narrowed, pulling the front onshore (Fig. 11f). This narrowing of overturning circulation is not due to wave streaming, which stays nearly the same with different stratification (Fig. 11e). Instead, the narrowing is linked to the downwelling (Fig. 11b, green arrow) beneath the front. The front is intensified with increasing stratification (Fig. 11f), and so is the downwelling. The intensified downwelling makes the inner-shelf surface water sink fast and thus shortens the offshore displacement completed by the surface water at the time of sinking to the bottom. This narrows the inner-shelf overturning circulation.

b. No wave streaming

To highlight wave-streaming effects, we design a comparison experiment in which wave streaming is deactivated by turning off wave bottom dissipation. Without wave streaming, the inner shelf no longer has the bottom onshore current (Fig. 12a) and overturning circulation (Fig. 12b). In addition, because wave bottom dissipation is turned off, wave energy is dissipated only by depth-induced breaking,

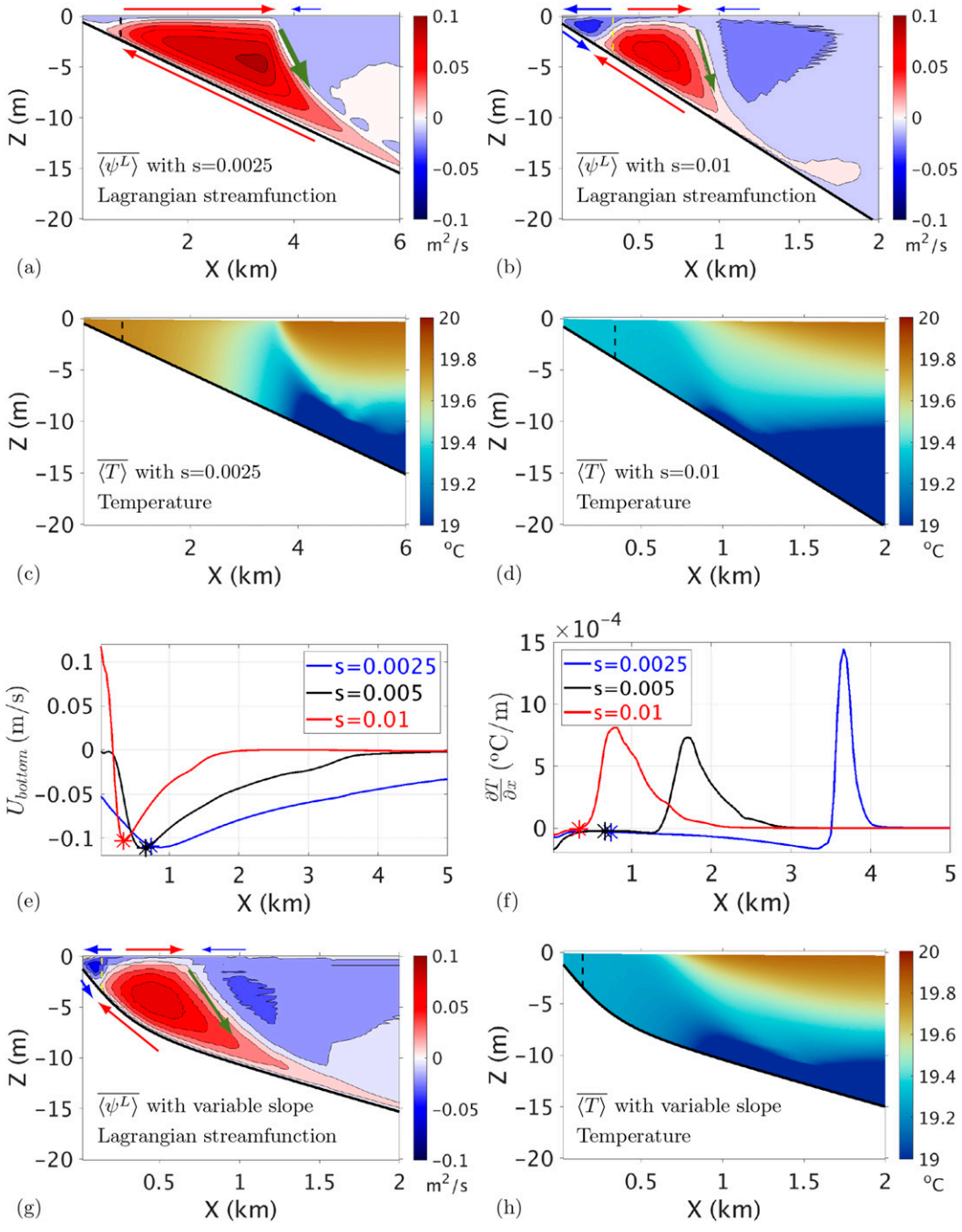

FIG. 10. Sensitivity to shelf slopes: Lagrangian streamfunction with shelf slope s = (a) 0.0025 and (b) 0.01. The arrows indicate directions of Lagrangian currents. Temperature with shelf slope s = (c) 0.0025 and (d) 0.01. Note that the x-axis range differs between (a) and (b) and between (c) and (d). Alongshore-averaged (e) bottom cross-shelf Eulerian velocity and (f) surface cross-shelf temperature gradient. (g) Lagrangian streamfunction and (h) temperature, with a more realistic shelf slope that decreases from 0.02 in the surf zone to 0.002 in the far offshore. Streamline jitters in (b) and (g) are due to computational errors. A temporal average is made over the second day. The dashed lines in (a)–(d), (g), and (h) and the asterisks in (e) and (f) mark the surf-zone edge.

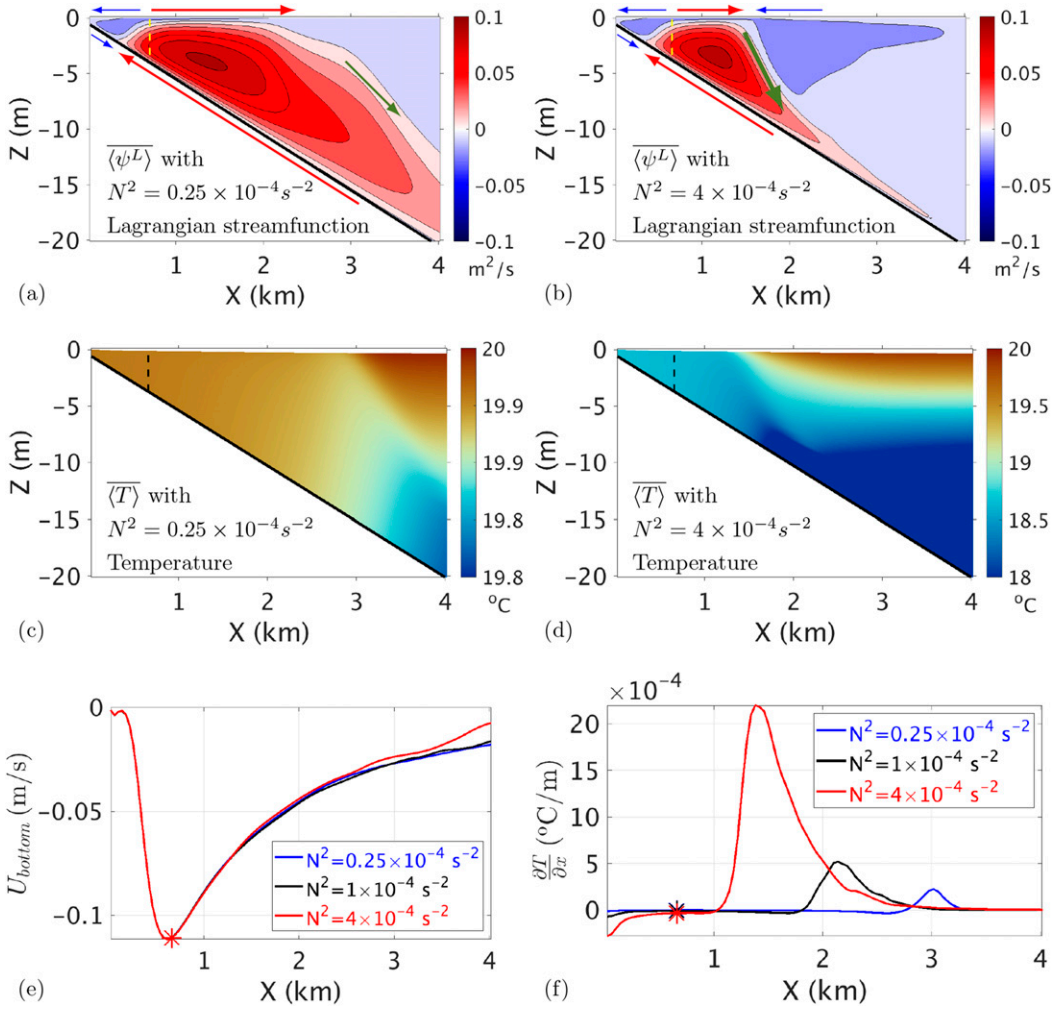

FIG. 11. Sensitivity to stratification: Lagrangian streamfunction with initial stratification N^2 = (a) 0.25×10^{-4} and (b) $4 \times 10^{-4}\,s^{-2}$. The arrows indicate directions of Lagrangian currents. Temperature with initial stratification N^2 = (c) 0.25×10^{-4} and (d) $4 \times 10^{-4}\,s^{-2}$. Note that the scale of the temperature color bar differs between (c) and (d). Alongshore-averaged (e) bottom cross-shelf Eulerian velocity and (f) surface cross-shelf temperature gradient. A temporal average is made over the second day. The dashed lines in (a)–(d) and the asterisks in (e) and (f) mark the surf-zone edge.

resulting in a stronger surf-zone circulation than that with wave streaming (Fig. 3b).

Without wave streaming, the inner-shelf vertical eddy viscosity is greatly reduced (Fig. 12c), smaller by a factor of approximately $O(10)$ than that with wave streaming (Fig. 3c). Nonetheless, wave breaking still increases the surf-zone eddy viscosity, causing differential mixing between the inside and outside of the surf zone. This gives rise to a front around the surf-zone edge (Fig. 12d; $x \approx 1$ km), called "wave-breaking front." Its strength is only about 1/7 of that of the farther offshore, wave-streaming front (Fig. 3d; $x \approx 2$ km).

Kumar and Feddersen (2017) also report a wave-breaking front caused by alongshore-variable wave breaking, and the front lies between two Lagrangian overturning circulations that are located in the surf zone and inner shelf. Nevertheless, although they include wave bottom dissipation, they ignore the wave streaming, missing its induced overturning circulation and front. In the nearshore, however, surfaces waves are usually subject to bottom drag, inducing wave streaming. Hence, the wave-streaming front is expected, and because of its larger strength, it is likely to dominate over the wave-breaking front.

c. *Tide included*

Tides are common in the nearshore and they can shift positions of the surf zone and inner shelf onshore/offshore by changing the sea level height (Masselink and Short 1993). Also, tidal currents enhance vertical mixing, leading to a tidal mixing front (Simpson and Hunter 1974). Then, how do tides modify the wave-streaming-induced overturning circulation and front? Here we provide a first glimpse of this question. We adopt analytic, semidiurnal barotropic tides at the offshore boundary. The tidal range is 4 m; to avoid dry cells at

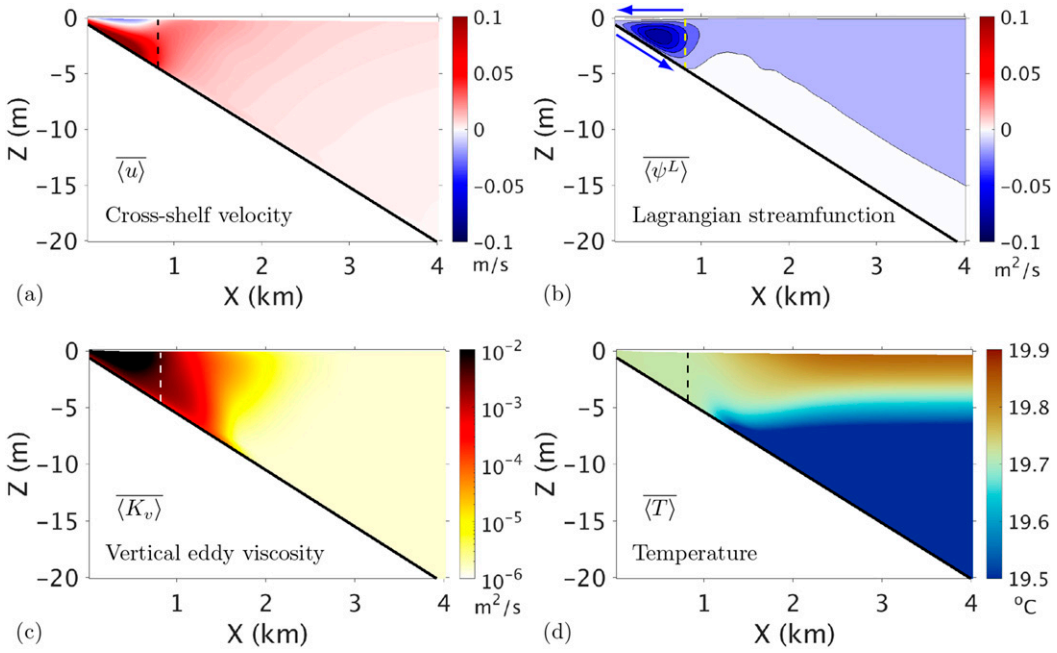

FIG. 12. Without wave streaming (cf. Fig. 3 with wave streaming): (a) cross-shelf Eulerian velocity, (b) Lagrangian streamfunction (the arrows indicate directions of Lagrangian currents), (c) vertical eddy viscosity, and (d) temperature. Note that the scale of the temperature color bar differs from that in Fig. 3. A temporal average is made over the second day. The dashed lines mark the surf-zone edge.

low tide, the shoreline is shifted offshore by 0.4 km. The tidal current is nearly equal to the wave streaming in magnitude, making the case most interesting. If the tidal current is too weak or too strong relative to the wave streaming, the strong one dominates and rules the inner-shelf circulation.

With tides the wave streaming drives a tidally averaged, inner-shelf Lagrangian overturning circulation (Fig. 13a). This overturning circulation is weakened by tides in comparison with that without tides (Fig. 3b), however, because the wave streaming is reduced by tides (Fig. 13d).

Tidal current and wave streaming together enhance the vertical eddy viscosity (Fig. 13b), making the inner-shelf vertical viscosity larger than that without tides (Fig. 3c). The larger viscosity causes more mixing, making the inner-shelf stratification weaker than that without tides. With weaker stratification, as explained in section 4, the inner-shelf overturning circulation becomes wider.

The enhanced mixing in the inner shelf also results in a front (Fig. 13c; $x \approx 2.5$ km) in contrast to the offshore weak mixing. The front arises from the mutual action of tidal current and wave streaming. Relative to the front without tides (Fig. 3d), this front is weaker and wider (Fig. 13e) and is pushed farther offshore by the wider inner-shelf overturning circulation. Still, it is unstable and generates shelf eddies.

In addition to the above tidally averaged results, there are also interesting results at instant moments due to the change of tidal current and sea level in each tidal cycle. For example, when the tidal current reaches its maximum, the wave-streaming overturning circulation disappears at that moment. Nevertheless, the front always exists because it can be maintained by either tidal current alone or wave streaming alone. Furthermore, the rising sea level during flood tides moves the overturning circulation and front onshore by several hundreds of meters, and, conversely, the falling sea level during ebb tides moves the overturning circulation and front offshore by several hundreds of meters.

d. *Wind included*

Winds are a common driving force to ocean circulation. Then, how do winds modify the wave-streaming-induced overturning circulation and front? Here we give a first glance at this question. We add a constant wind stress of 0.03 N m^{-2} in the cross-shelf direction, which drives a current comparable to the wave streaming in magnitude.

Because of the wind, a surface boundary layer forms, about 10 m deep, and extends from the inner shelf till the offshore boundary. In the inner shelf, it overlaps with the bottom boundary layer created by wave streaming. In both boundary layers, the vertical eddy viscosity is enhanced and has similar values.

An offshore-directed wind drives an overturning circulation across the surface boundary layer (Fig. 14a), next to the surf-zone overturning circulation generated by wave breaking. The water inside the wind-driven overturning circulation is well mixed due to enhanced vertical viscosity. This makes the temperature nearly uniform within the surface boundary layer (Fig. 14b).

Wave streaming again induces an overturning circulation in the inner shelf, pushing the wind-driven overturning circulation offshore (Fig. 14c). Also, wave streaming pumps up

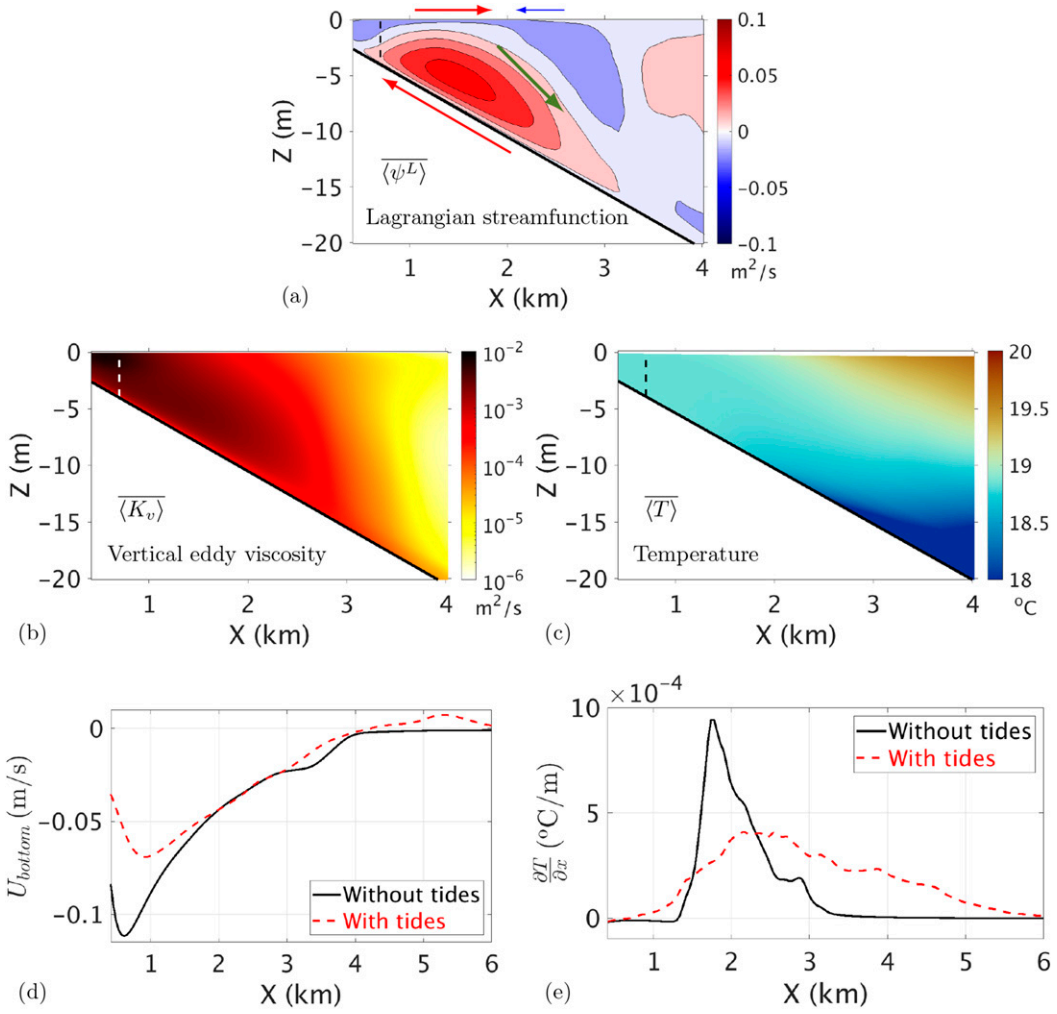

FIG. 13. With tides: (a) Lagrangian streamfunction (the arrows indicate directions of Lagrangian currents), (b) vertical eddy viscosity, (c) temperature, and alongshore-averaged (d) bottom cross-shelf Eulerian velocity and (e) surface cross-shelf temperature gradient. A temporal (tidal) average is made over the second day. The dashed lines in (a)–(c) mark the surf-zone edge.

deep and cold water into its induced overturning circulation, creating a front between the water inside and outside the overturning circulation (Fig. 14d; $x \approx 2$ km). The frontal strength is similar to that without winds, and the front is also unstable and generates shelf eddies. Nonetheless, the shelf eddies are weakened by Langmuir circulation[3] that appears because of the wind.

By contrast, an onshore-directed wind drives an overturning circulation in opposite direction to the wave-streaming overturning circulation (Fig. 14e). This considerably suppresses the wave-streaming overturning circulation and its capability of bringing up deep and cold water. Thus, the wave-streaming front is reduced dramatically (Fig. 14f; $x \approx 2$ km), and as a result, the frontal instability cannot develop.

5. Conclusions

We demonstrate a nearshore front induced by wave streaming. Horizontally the wave-streaming front is parallel to the shore, and vertically it extends from the surface to the bottom. Wave streaming plays two roles in the frontogenesis. First, wave streaming drives an inner-shelf Lagrangian overturning circulation and pumps up deep and cold water into the overturning circulation. The water inside the overturning circulation is rapidly mixed and cooled because of the wave-streaming-enhanced viscosity. However, the offshore water outside the overturning circulation remains stratified and warmer. Hence, a front develops between the water inside and outside the overturning circulation. Second, to balance the onshore transport by bottom wave streaming, the inner-shelf offshore current is intensified near the surface,

[3] Our hydrostatic, coupled wave–circulation model can partly resolve large-scale Langmuir circulation that is $O(1)$ km long, $O(100)$ m wide, and $O(10)$ m deep. The small aspect ratio (~0.1) justifies the hydrostatic approximation.

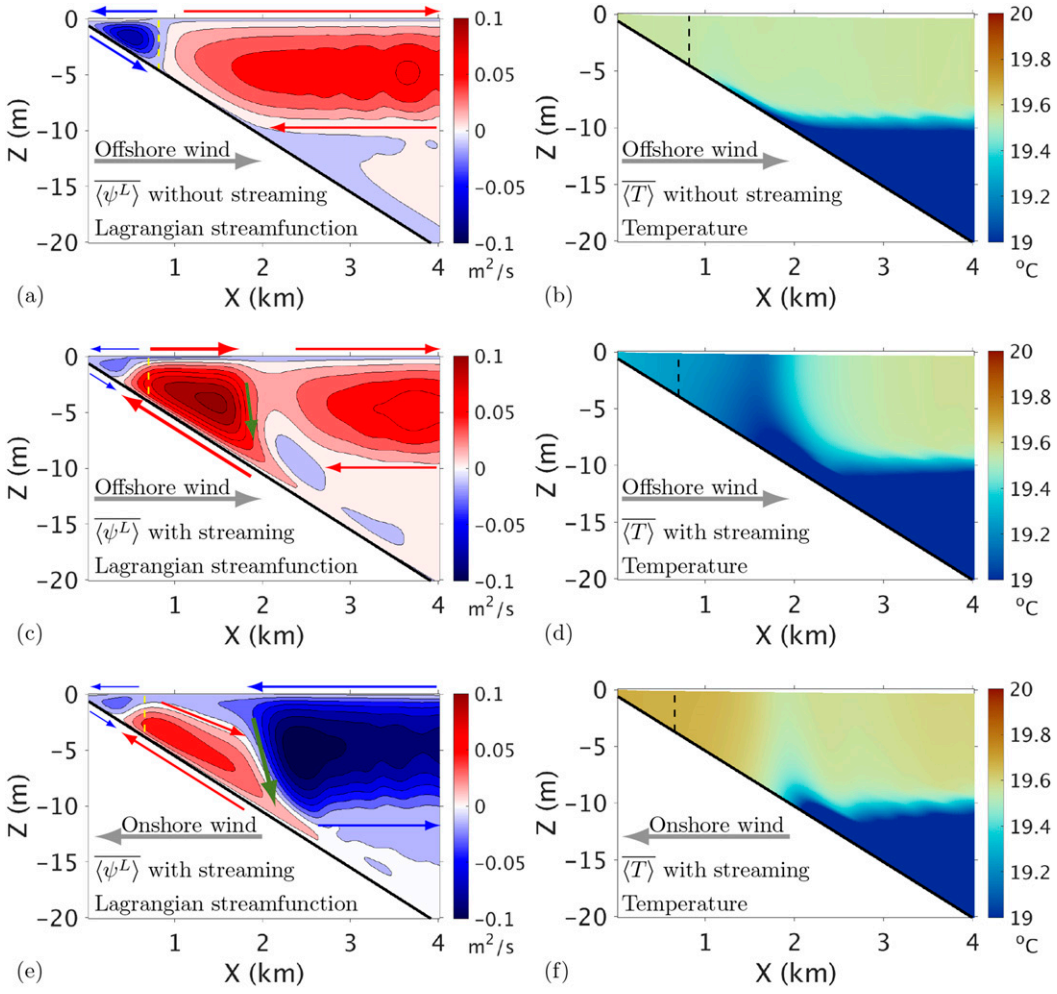

FIG. 14. With winds: (left) Lagrangian streaming function and (right) temperature for (a),(b) offshore wind without wave streaming; (c),(d) offshore wind with wave streaming; and (e),(f) onshore wind with wave streaming. The gray arrows denote wind directions, and other arrows in (a), (c), and (e) indicate directions of Lagrangian currents. A temporal average is made over the second day. The dashed lines mark the surf-zone edge.

sharpening the surface front. The schematic Fig. 15 outlines wave-streaming effects on the nearshore ocean circulation.

The wave-streaming front destabilizes at the surface and generates submesoscale shelf eddies spreading offshore. The frontal instability is accelerated by surf eddies that are able to reach and perturb the front. Using shore-released passive tracers, we show that shelf eddies cause the offshore transport across the front. Particularly, after crossing the front into the offshore, tracers are concentrated below the surface.

Sensitivities of the wave-streaming front are examined with respect to the wave energy, bottom roughness, shelf slope, and stratification. As the wave energy or bottom roughness increases, the wave-streaming overturning circulation expands offshore, pushing the front offshore. As the shelf slope or stratification increases, the overturning circulation narrows onshore, pulling the front onshore.

In the presence of tides, wave streaming drives a tidally averaged, inner-shelf Lagrangian overturning circulation and an associated front. In fact, the front is generated by the mutual action of wave streaming and tides. In comparison with the case without tides, both the overturning circulation and the front are wider and weaker, and they are shifted back and forth in the cross-shelf direction due to the sea level change in each tidal cycle.

With offshore-directed winds, wave streaming can still induce an inner-shelf overturning circulation and an associated front. With onshore-directed winds, however, the overturning circulation and front are suppressed remarkably by an onshore wind-driven overturning circulation that is opposite to the wave-streaming overturning circulation.

The wave-streaming-induced overturning circulation and front play an important role in regulating the cross-shelf transport among the surf zone, inner shelf and the farther offshore, especially when tides and winds are negligible or weak relative to the wave streaming. The wave-streaming overturning circulation connects the inner shelf with the surf

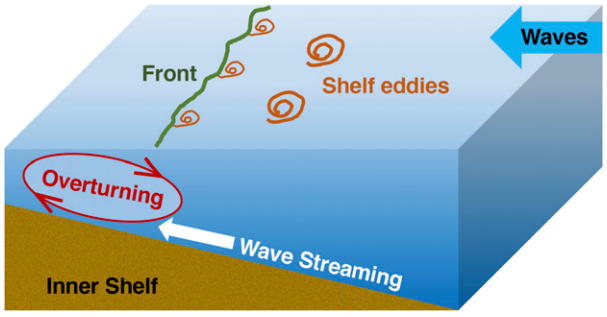

FIG. 15. A schematic illustration of the wave-streaming-induced Lagrangian overturning circulation and front in the inner shelf, as well as offshore-spreading shelf eddies generated by the frontal instability.

zone and promotes material exchange between the two regions (Wang et al. 2020). For example, wave streaming can transport near-bottom fish larvae from the inner shelf to the surf zone (Shanks et al. 2015; Fujimura et al. 2018). On the other hand, the overturning circulation can bring surf-zone fish larvae to the inner shelf. Therefore, some marine species may utilize the overturning circulation to help them migrate between the surf zone and inner shelf.

The wave-streaming front acts as a barrier that limits the cross-shelf transport between the inner shelf and the farther offshore, though frontal instabilities and shelf eddies can break the frontal barrier. Once materials such as plankton and nutrients cross the front into the offshore, they are likely to concentrate below the surface. That is, in the offshore next to the front, the subsurface layer may contain a higher concentration of some plankton and may show a higher biological production than the surface.

In brief, wave streaming and its induced front and overturning circulation modify the nearshore ocean circulation, regulate the cross-shelf transport, and further affect the ecosystem's health. Hence, we call for more attention to the wave streaming, in both numerical simulations and field observations.

Acknowledgments. Authors Wang and McWilliams are grateful for the support of the Office of Naval Research (N00014-15-1-2645) and the National Science Foundation (OCE-1355970). Author Uchiyama appreciates the support of Japan Society for the Promotion of Science (JSPS) Grants-in-Aid for Scientific Research (18H03798) at Kobe University. The numerical experiments are done at the Extreme Science and Engineering Discovery Environment (XSEDE). The authors also appreciate helpful suggestions from two anonymous reviewers.

Data availability statement. The dataset on which this paper is based is too large to be retained or publicly archived with available resources. Documentation and methods used to support this study are available from the corresponding author Peng Wang at the University of California, Los Angeles.

APPENDIX

Parameterizations of Nonconservative Wave Forces

The wave breaking dissipation ε^b is determined by the parameterization (Church and Thornton 1993),

$$\varepsilon^b = \frac{3\sqrt{\pi}}{16}\rho_0 g \frac{B_b^3 \sigma}{2\pi D} H_{\rm rms}^3 \left\{1 + \tanh\left[8\left(\frac{H_{\rm rms}}{\gamma_b D} - 1\right)\right]\right\} \times \left\{1 - \left[1 + \left(\frac{H_{\rm rms}}{\gamma_b D}\right)^2\right]^{-5/2}\right\}, \quad \text{(A1)}$$

where ρ_0 is the water density, g is the gravitational acceleration, D is the water depth, $H_{\rm rms}$ is the RMS wave height, B_b and γ_b are constants, σ is the wave intrinsic frequency, and k is the wavenumber. The wave breaker force is then given by

$$\mathbf{F}^b = (\varepsilon^b/\sigma)\mathbf{k}. \quad \text{(A2)}$$

The wave bottom dissipation ε^f is determined by the parameterization (Reniers et al. 2004),

$$\varepsilon^f = \frac{1}{2\sqrt{\pi}}\rho_0 f_w |\mathbf{u}_{\rm orb}^w|^3, \quad \text{(A3)}$$

where $f_w = 1.39(\sigma z_o/|\mathbf{u}_{\rm orb}^w|)^{0.52}$ is the wave friction factor (Soulsby 1997), z_o is the bottom roughness height, $|\mathbf{u}_{\rm orb}^w| = \sigma H_{\rm rms}/[2\sinh(kD)]$ is the near-bottom wave orbital velocity, $H_{\rm rms}$ is the RMS wave height, and D is the water depth. The wave-streaming force is then given by

$$\mathbf{F}^f = (\varepsilon^f/\sigma)\mathbf{k}. \quad \text{(A4)}$$

Surface waves enhance bottom drag on currents, and this drag is parameterized as (Feddersen et al. 2000)

$$\mathbf{F}^d = 0.015\rho_0 \left(\frac{k_a}{D}\right)^{1/3} \left[(1.16)^2 + \left(\frac{|\mathbf{u}|}{|\mathbf{u}_{\rm rms}^w|}\right)^2\right]^{1/2} |\mathbf{u}_{\rm rms}^w|\mathbf{u}, \quad \text{(A5)}$$

where $\mathbf{u}_{\rm rms}^w = \mathbf{u}_{\rm orb}^w/\sqrt{2}$ is the RMS near-bottom wave orbital velocity and $k_a = 0.0125$ m is apparent roughness height (Ruessink et al. 2001).

REFERENCES

Akan, Ç., J. C. McWilliams, and Y. Uchiyama, 2020: Topographic and coastline influences on surf eddies. *Ocean Model.*, **147**, 101565, https://doi.org/10.1016/j.ocemod.2019.101565.

Allen, J., P. Newberger, and J. Federiuk, 1995: Upwelling circulation on the Oregon continental shelf. Part I: Response to idealized forcing. *J. Phys. Oceanogr.*, **25**, 1843–1866, https://doi.org/10.1175/1520-0485(1995)025<1843:UCOTOC>2.0.CO;2.

Austin, J. A., and S. J. Lentz, 2002: The inner shelf response to wind-driven upwelling and downwelling. *J. Phys. Oceanogr.*, **32**, 2171–2193, https://doi.org/10.1175/1520-0485(2002)032<2171:TISRTW>2.0.CO;2.

Brink, K. H., 2016: Cross-shelf exchange. *Annu. Rev. Mar. Sci.*, **8**, 59–78, https://doi.org/10.1146/annurev-marine-010814-015717.

Brown, J. A., J. H. MacMahan, A. J. Reniers, and E. B. Thornton, 2015: Field observations of surf zone–inner shelf exchange on a rip-channeled beach. *J. Phys. Oceanogr.*, **45**, 2339–2355, https://doi.org/10.1175/JPO-D-14-0118.1.

Chapman, D. C., and S. J. Lentz, 1994: Trapping of a coastal density front by the bottom boundary layer. *J. Phys. Oceanogr.*, **24**, 1464–1479, https://doi.org/10.1175/1520-0485(1994)024<1464:TOACDF>2.0.CO;2.

Chen, C., R. J. Schlitz, R. G. Lough, K. W. Smith, R. Beardsley, and J. P. Manning, 2003: Wind-induced, cross-frontal exchange on Georges Bank: A mechanism for early summer on-bank biological particle transport. *J. Geophys. Res.*, **108**, 8011, https://doi.org/10.1029/2002JC001358.

Church, J. C., and E. B. Thornton, 1993: Effects of breaking wave induced turbulence within a longshore current model. *Coastal Eng.*, **20**, 1–28, https://doi.org/10.1016/0378-3839(93)90053-B.

Cushman-Roisin, B., and J.-M. Beckers, 2011: *Introduction to Geophysical Fluid Dynamics: Physical and Numerical Aspects*. Academic Press, 875 pp.

Feddersen, F., R. Guza, S. Elgar, and T. Herbers, 2000: Velocity moments in alongshore bottom stress parameterizations. *J. Geophys. Res.*, **105**, 8673–8686, https://doi.org/10.1029/2000JC900022.

Fujimura, A. G., A. J. Reniers, C. B. Paris, A. L. Shanks, J. H. MacMahan, and S. G. Morgan, 2018: Mechanisms of cross-shore transport and spatial variability of phytoplankton on a rip-channeled beach. *Front. Mar. Sci.*, **5**, 183, https://doi.org/10.3389/fmars.2018.00183.

Gawarkiewicz, G., K. H. Brink, F. Bahr, R. C. Beardsley, M. Caruso, J. F. Lynch, and C.-S. Chiu, 2004: A large-amplitude meander of the shelfbreak front during summer south of New England: Observations from the shelfbreak primer experiment. *J. Geophys. Res.*, **109**, C03006, https://doi.org/10.1029/2002JC001468.

Hoskins, B. J., 1982: The mathematical theory of frontogenesis. *Annu. Rev. Fluid Mech.*, **14**, 131–151, https://doi.org/10.1146/annurev.fl.14.010182.001023.

Houghton, R., F. Aikman III, and H. Ou, 1988: Shelf-slope frontal structure and cross-shelf exchange at the New England shelf-break. *Cont. Shelf Res.*, **8**, 687–710, https://doi.org/10.1016/0278-4343(88)90072-6.

Kranenburg, W. M., J. S. Ribberink, R. E. Uittenbogaard, and S. J. Hulscher, 2012: Net currents in the wave bottom boundary layer: On waveshape streaming and progressive wave streaming. *J. Geophys. Res.*, **117**, F03005, https://doi.org/10.1029/2011JF002070.

Kumar, N., and F. Feddersen, 2017: The effect of Stokes drift and transient rip currents on the inner shelf. Part II: With stratification. *J. Phys. Oceanogr.*, **47**, 243–260, https://doi.org/10.1175/JPO-D-16-0077.1.

Large, W. G., J. C. McWilliams, and S. C. Doney, 1994: Oceanic vertical mixing: A review and a model with a nonlocal boundary layer parameterization. *Rev. Geophys.*, **32**, 363–403, https://doi.org/10.1029/94RG01872.

Lentz, S. J., and M. R. Fewings, 2012: The wind-and wave-driven inner-shelf circulation. *Annu. Rev. Mar. Sci.*, **4**, 317–343, https://doi.org/10.1146/annurev-marine-120709-142745.

——, M. Fewings, P. Howd, J. Fredericks, and K. Hathaway, 2008: Observations and a model of undertow over the inner continental shelf. *J. Phys. Oceanogr.*, **38**, 2341–2357, https://doi.org/10.1175/2008JPO3986.1.

Longuet-Higgins, M. S., 1953: Mass transport in water waves. *Philos. Trans. Roy. Soc. London*, **245A**, 535–581, https://doi.org/10.1098/rsta.1953.0006.

MacMahan, J. H., E. B. Thornton, and A. J. Reniers, 2006: Rip current review. *Coastal Eng.*, **53**, 191–208, https://doi.org/10.1016/j.coastaleng.2005.10.009.

Marchesiello, P., R. Benshila, R. Almar, Y. Uchiyama, J. C. McWilliams, and A. Shchepetkin, 2015: On tridimensional rip current modeling. *Ocean Modell.*, **96**, 36–48, https://doi.org/10.1016/j.ocemod.2015.07.003.

Masselink, G., and A. D. Short, 1993: The effect of tide range on beach morphodynamics and morphology: A conceptual beach model. *J. Coastal Res.*, **9**, 785–800.

McWilliams, J. C., 2018: Surface wave effects on submesoscale fronts and filaments. *J. Fluid Mech.*, **843**, 479–517, https://doi.org/10.1017/jfm.2018.158.

——, 2021: Oceanic frontogenesis. *Annu. Rev. Mar. Sci.*, **13**, 227–253, https://doi.org/10.1146/annurev-marine-032320-120725.

——, J. M. Restrepo, and E. M. Lane, 2004: An asymptotic theory for the interaction of waves and currents in coastal waters. *J. Fluid Mech.*, **511**, 135–178, https://doi.org/10.1017/S0022112004009358.

Nittrouer, C. A., and L. D. Wright, 1994: Transport of particles across continental shelves. *Rev. Geophys.*, **32**, 85–113, https://doi.org/10.1029/93RG02603.

Pineda, J., 1994: Internal tidal bores in the nearshore: Warm-water fronts, seaward gravity currents and the onshore transport of neustonic larvae. *J. Mar. Res.*, **52**, 427–458, https://doi.org/10.1357/0022240943077046.

Reniers, A., E. Thornton, T. Stanton, and J. Roelvink, 2004: Vertical flow structure during sandy duck: Observations and modeling. *Coastal Eng.*, **51**, 237–260, https://doi.org/10.1016/j.coastaleng.2004.02.001.

Reniers, A. J., J. MacMahan, E. Thornton, T. Stanton, M. Henriquez, J. Brown, J. Brown, and E. Gallagher, 2009: Surf zone surface retention on a rip-channeled beach. *J. Geophys. Res.*, **114**, C10010, https://doi.org/10.1029/2008JC005153.

Romero, L., D. Hypolite, and J. C. McWilliams, 2020: Submesoscale current effects on surface waves. *Ocean Model.*, **153**, 101662, https://doi.org/10.1016/j.ocemod.2020.101662.

Ruessink, B., J. Miles, F. Feddersen, R. Guza, and S. Elgar, 2001: Modeling the alongshore current on barred beaches. *J. Geophys. Res.*, **106**, 22 451–22 463, https://doi.org/10.1029/2000JC000766.

Shanks, A. L., 1983: Surface slicks associated with tidally forced internal waves may transport pelagic larvae of benthic invertebrates and fishes shoreward. *Mar. Ecol. Prog. Ser.*, **13**, 311–315, https://doi.org/10.3354/meps013311.

——, J. MacMahan, S. G. Morgan, A. J. M. Reniers, M. Jarvis, J. Brown, A. Fujimura, and C. Griesemer, 2015: Transport of larvae and detritus across the surf zone of a steep reflective pocket beach. *Mar. Ecol. Prog. Ser.*, **528**, 71–86, https://doi.org/10.3354/meps11223.

Simpson, J., and J. Hunter, 1974: Fronts in the Irish sea. *Nature*, **250**, 404–406, https://doi.org/10.1038/250404a0.

Soulsby, R., 1997: *Dynamics of Marine Sands: A Manual for Practical Applications*. Thomas Telford, 249 pp.

Sullivan, P. P., and J. C. McWilliams, 2019: Langmuir turbulence and filament frontogenesis in the oceanic surface boundary layer. *J. Fluid Mech.*, **879**, 512–553, https://doi.org/10.1017/jfm.2019.655.

Suzuki, N., and B. Fox-Kemper, 2016: Understanding Stokes forces in the wave-averaged equations. *J. Geophys. Res. Oceans*, **121**, 3579–3596, https://doi.org/10.1002/2015JC011566.

——, ——, P. E. Hamlington, and L. P. Van Roekel, 2016: Surface waves affect frontogenesis. *J. Geophys. Res. Oceans*, **121**, 3597–3624, https://doi.org/10.1002/2015JC011563.

Trowbridge, J., and O. S. Madsen, 1984: Turbulent wave boundary layers: 2. Second-order theory and mass transport. *J. Geophys. Res.*, **89**, 7999–8007, https://doi.org/10.1029/JC089iC05p07999.

Uchiyama, Y., J. C. McWilliams, and A. F. Shchepetkin, 2010: Wave–current interaction in an oceanic circulation model with a vortex-force formalism: Application to the surf zone. *Ocean Modell.*, **34**, 16–35, https://doi.org/10.1016/j.ocemod.2010.04.002.

——, ——, and C. Akan, 2017: Three-dimensional transient rip currents: Bathymetric excitation of low-frequency intrinsic variability. *J. Geophys. Res. Oceans*, **122**, 5826–5849, https://doi.org/10.1002/2017JC013005.

Wang, P., and T. M. Özgökmen, 2018: Langmuir circulation with explicit surface waves from moving-mesh modeling. *Geophys. Res. Lett.*, **45**, 216–226, https://doi.org/10.1002/2017GL076009.

——, J. McWilliams, Y. Uchiyama, M. Chekroun, and D. Yi, 2020: Effects of wave streaming and wave variations on nearshore wave-driven circulation. *J. Phys. Oceanogr.*, **50**, 3025–3041, https://doi.org/10.1175/JPO-D-19-0304.1.

Weber, J. E. H., G. Broström, and Ø. Saetra, 2006: Eulerian versus Lagrangian approaches to the wave-induced transport in the upper ocean. *J. Phys. Oceanogr.*, **36**, 2106–2118, https://doi.org/10.1175/JPO2951.1.

Xu, Z., and A. Bowen, 1994: Wave-and wind-driven flow in water of finite depth. *J. Phys. Oceanogr.*, **24**, 1850–1866, https://doi.org/10.1175/1520-0485(1994)024<1850:WAWDFI>2.0.CO;2.